Current Induced Tilting of Domain Walls in High Velocity Motion along Perpendicularly Magnetized Micron-Sized Co/Ni/Co Racetracks

To cite this article: Kwang-Su Ryu *et al* 2012 *Appl. Phys. Express* **5** 093006

Applied Physics Express 5 (2012) 093006
http://dx.doi.org/10.1143/APEX.5.093006

Current Induced Tilting of Domain Walls in High Velocity Motion along Perpendicularly Magnetized Micron-Sized Co/Ni/Co Racetracks

Kwang-Su Ryu, Luc Thomas*, See-Hun Yang, and Stuart S. P. Parkin

IBM Almaden Research Center, San Jose, CA 95120, U.S.A.

Received August 9, 2012; accepted August 22, 2012; published online September 6, 2012

Kerr microscopy is used to investigate domain wall motion in response to nanosecond-long current pulses in perpendicularly magnetized micron-sized Co/Ni/Co racetracks. Domain wall velocities greater than 300 m/s are observed. The velocity is independent of the pulse length for a wide range of current densities. However, the domain wall dynamics depends on the pulse length just above the threshold current for motion, where slow creep motion occurs, and at very high current densities, where domain nucleation takes place. We also observe a tilting of the domain wall that cannot be accounted for by the Oersted field from the driving current.

The current-controlled manipulation and motion of magnetic domain walls (DWs)[1–6] in nanowires[7–11] is key to various memory[12,13] and logic[14] devices currently under investigation. One such device is the Racetrack Memory,[12] a novel memory storage device in which data are stored and accessed by moving a series of DWs along magnetic wires — the racetracks. Series of DWs are moved in lockstep by passing pulses of spin-polarized current along the racetracks.[15] The performance of the device, namely, its storage density, power consumption, and data rate, depend especially on the width of the DWs and the speed at which these DWs can be moved with current for a given current density. Materials with perpendicular magnetic anisotropy (PMA) support very narrow DWs. Moreover, very low critical current densities[16,17] and extremely high current-driven DW velocities[18] have been reported in PMA wires. This makes PMA materials excellent candidates for Racetrack Memory.[19]

In this letter, we report very fast current-driven DW motion in Co/Ni/Co racetracks with PMA. We show that the DW velocity is essentially independent of the current pulse length for a wide range of current densities. By contrast, the DW motion depends strongly on the pulse length at low current densities, just above the critical current density for DW motion, and at very high current densities, at which current-induced nucleation of reversed domains becomes prevalent. We also show that the critical current density and DW velocity are largely independent of the width of the racetrack for widths between 2 and 20 μm.

The devices were fabricated by ultraviolet photolithography and argon ion milling from blanket films deposited by magnetron sputtering on silicon wafers covered by a 25-nm-thick SiO_2 layer. The composition of the stack is 20 TaN/15 Pt/3 Co/7 Ni/1.5 Co/50 TaN (all thicknesses are in angstroms). The blanket films exhibit very good PMA. The saturation magnetization and anisotropy constant are found from superconducting quantum interference device (SQUID) magnetometry to be $M_S \sim 600\,\mathrm{emu/cm^3}$ and $K \sim 5.9 \times 10^6\,\mathrm{erg/cm^3}$, respectively. Current-driven DW motion is studied in devices such as the one shown in Fig. 1(a). The wire in the central portion of the device, where DW motion is studied, is 50 μm long. Its width is varied between 2 and 20 μm. This wire is connected at both ends to wider regions that are used as bond pads for electrical connections. In most cases, we find that the PMA is significantly reduced at the wire bonds,

*E-mail address: lucthom@us.ibm.com

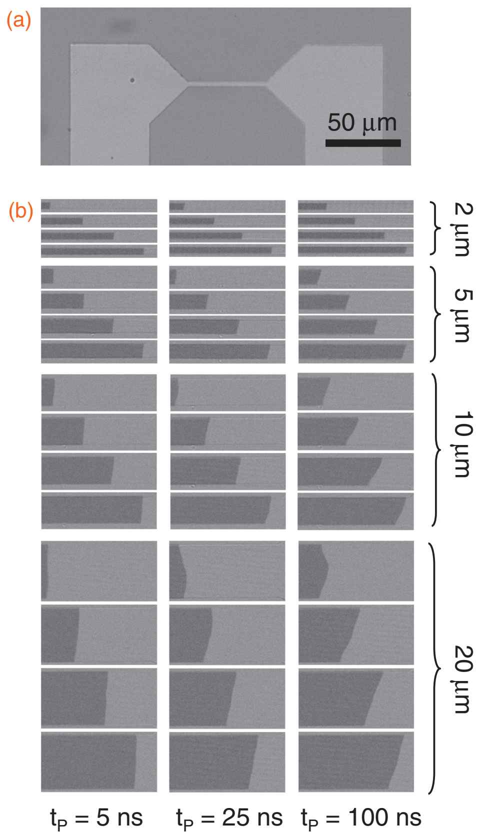

Fig. 1. (a) Optical image of a typical device. DW motion is studied in the 50-μm-long narrow wire in the central part of the device. (b) Kerr microscopy images showing DW motion in response to a series of positive current pulses having a current density of $\sim 1.1 \times 10^8\,\mathrm{A/cm^2}$. The width of the devices and the current pulse lengths are indicated in the figure. The numbers of pulses applied between consecutive images are 24, 4, and 1 for 5-, 25-, and 100-ns-long pulses, respectively. Note that in some cases (for example, for the 20-μm-wide device), the DW is curved rather than tilted in the early stages of its motion. This is because the DW is positioned at the left end of the wire with a negative current pulse prior to these experiments. Thus, the DW can be tilted in the opposite direction in its initial state, leading to the observed curved shape at the beginning of its motion under positive currents.

such that DWs are nucleated near the bonds and can propagate in the wire under an external field. Once a single DW is injected in the wire, the field is reduced to zero and DW motion is studied by applying a series of current pulses of length t_P, which vary between 5 and 100 ns, to the device.

Kerr microscopy in differential mode is used to monitor the position of a DW in the wire in response to a series of current pulses. Sequences of images recorded for different wire widths w and pulse lengths t_P are shown in Fig. 1(b). In these experiments, the current density J is $\sim 1.1 \times 10^8$ A/cm^2. The number of pulses n between two saved images is adjusted such that the DW moves by a similar distance ($n = 1$, 4, and 24 for $t_P = 100$, 25, and 5 ns, respectively). The time between consecutive pulses is 10 ms. An additional waiting time of 550 ms is used when images are saved to allow the time averaging of the Kerr signal. In these samples, DWs move in the direction of the current that flows from left to right for positive current. The Kerr contrast is determined by the magnetization direction of the domain that expands as a result of the motion of the DW (the black contrast seen in these images corresponds to domain magnetization pointing into the plane of the paper). Two observations can be made from these sets of experiments. First, the DW moves approximately the same distance for the same integrated time ($= n \times t_p$) for which the current is applied, independent of the length of the individual current pulses and independent of the wire width. Second, the DW is tilted as it moves along the wire, and the tilt angle increases significantly for longer pulses. As shown in Fig. 2(a), the tilt direction is reversed for positive and negative currents. It is also reversed when the orientation of the domains is reversed (i.e., for down/up or up/down DWs). The symmetry of the tilt is consistent with the effect of a perpendicular magnetic field pointing in opposite directions at opposite edges of the wires. The Oersted field created by the current pulse has this profile, and indeed, tilts have been attributed to the Oersted field in GaMnAs devices.[20,21] However, the tilt direction in our experiments is opposite to that caused by the Oersted field, suggesting that the tilt has another origin. Possible origins could include non-uniform current distributions in the vicinity of the DW due, for example, to the reversal of the anomalous Hall voltage at the DW[23] or non-uniform torques due to spin accumulation induced by the spin hall effect at the interface with the Pt layer.[24] Note that the value of the tilt angle is not only related to the dynamical deformations of the DW during its motion, but must also be dependent on quasi-static pinning. Indeed, no current is applied when the Kerr images are recorded between sets of pulses (other than a 5 μA dc current used to monitor the device resistance). This means that the lowest energy state for the DW should be that which minimizes its length, that is, that in which the DW takes up a straight line perpendicular to the edges of the wire. Without any pinning, the DW should relax rapidly to this lowest energy state and thus no tilt would be observed. In these devices, we find that the magnetic propagation field needed to overcome pinning in the wire is about 10 Oe, and is independent of the width of the device. The dependence of the tilt on t_P is shown in Fig. 2(b) for the four cases shown in Fig. 2(a). Positive numbers correspond to counterclockwise tilts. Data points and error bars are given by the average and standard deviation of the tilt angle, respectively, which are measured for DW displacements between 10 and 40 μm.

In order to quantify the effect of the current pulse length and wire width, the DW velocity is calculated from a series of images such as that shown in Fig. 1(b) by determining the DW position in each of the images using an automated analysis of the Kerr contrast along the wire. We use a linear

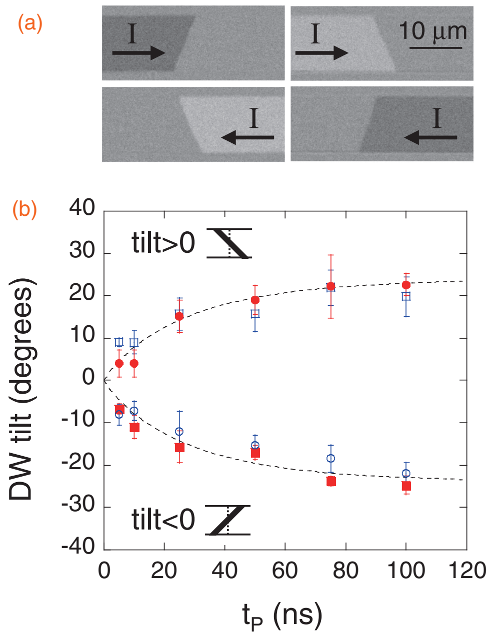

Fig. 2. (a) Kerr microscopy images of a 10-μm-wide device showing the tilt angle in response to 100-ns-long pulses having a current density of $\sim 1.0 \times 10^8$ A/cm^2. The current direction is indicated by the arrows. Images on the left (right)-hand side correspond to a down/up (up/down) DW. (b) Tilt angle versus pulse length for down/up (squares) and up/down (circles) DWs in response to current pulses of opposite polarities (solid and open symbols are for positive and negative currents, respectively). Dashed lines are guides to the eye. Positive and negative values of the tilt angle correspond to counterclockwise and clockwise rotations, respectively, as indicated by the schematic diagrams.

fit of the DW position versus the cumulative current pulse length t_{CP}, which is the product of t_P by the number of pulses applied to the device. The standard deviation of the differential velocity values calculated for all the points of the DW position vs t_{CP} curves is used as error bars for the velocity measurement. The variations of the DW velocity as a function of the current density J are shown in Fig. 3(a) for a 2-μm-wide device, for t_P between 5 and 100 ns. J is calculated from the device resistance by assuming uniform conduction in the metallic layers, which in this case have a total thickness of ~26.5 Å. DW motion faster than 300 m/s is observed. This value is comparable to those reported by Miron *et al.*[18] However, whereas these previous results were obtained for individual DW displacements limited to a few hundreds of nanometers, our data are measured for sustained DW motion over up to 50 μm [as shown in Fig. 1(b)]. Data shown in Fig. 3(a) for different values of t_P all fall on the same master curve, indicating that the current pulse length plays little role in the DW velocity. Note that the shape of this master curve is different from the results reported in the literature for PMA systems.[18,22,25] Indeed, these earlier results show that the slope of the velocity versus J curve decreases at high current densities. Our data also show this decrease at $\sim 2 \times 10^8$ A/cm^2, but we find an unusual increase of the slope for still higher current densities. The origin of this behavior is unclear. It does not seem to be related to the tilt of the DW observed in Fig. 1(b) since the shape of the curve is weakly dependent on t_P. Closer inspection of the data reveals that the pulse length plays a significant role only in the low and high

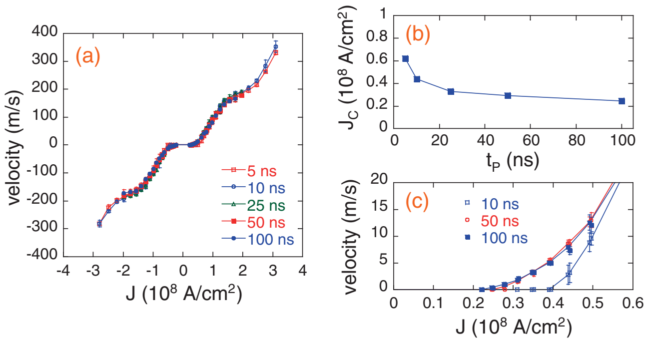

Fig. 3. (a) DW velocity versus current density for a 2-µm-wide device. (b) Critical current density for DW motion J_C as a function of the current pulse length t_P. (c) Details of the DW velocity vs current density curve highlighting the DW dynamics just above the critical current. This curve shows the absolute values of data taken for both current polarities.

current density regimes. In the low J limit, DW motion only occurs over significant distances when J exceeds a critical value J_C. As shown in Fig. 3(b), J_C decreases with t_P, from 6.2×10^7 A/cm^2 for $t_P = 5$ ns to 2.5×10^7 A/cm^2 for $t_P = 100$ ns. This decrease is associated with the onset of current-induced DW creep,[23,26] which takes place in the subthreshold limit for pulses longer than ~25 ns [Fig. 3(c)]. In the high J limit, DW motion is replaced by random nucleation of DWs, possibly due to Joule heating and magnetization reversal induced by the Oersted field from the current. This nucleation threshold J_N also depends on t_P. For $t_P = 5$ ns, no nucleation occurs below the current limit of our pulse generator (which corresponds to $J \sim 3 \times 10^8$ A/cm^2). By contrast, when $t_P = 100$ ns, nucleation occurs when J exceeds 2×10^8 A/cm^2.

The role played by the racetrack width w is shown in Fig. 4 for 2-, 5-, 10-, and 20-µm-wide devices. Panels (a), (b), and (c) show results for $t_P = 5$, 25, and 100 ns, respectively. Interestingly, for all three current pulse lengths, the DW velocity is almost independent of the device width, even though the current injected in the racetrack differs by a factor of 10. Small deviations from the data measured for $w = 2$ µm are only observed when the current density exceeds 1.75 and 1.5×10^8 A/cm^2 for $w = 10$ and 5 µm, respectively (note that for $w = 20$ µm, no deviation is observed in the experimentally accessible current range).

In summary, we have shown evidence from Kerr microscopy studies of the current-induced motion of individual DWs in 50-µm-long perpendicularly magnetized Co/Ni/Co racetracks that DWs can be moved at velocities higher than 300 m/s. The DW velocity is weakly dependent on the current pulse length over a wide range of current densities and can be varied continuously between 20 and 300 m/s by controlling the current density. In addition, we observe a tilting of the domain wall across the wire's width that increases with the length of the current pulse and cannot be accounted for by any Oersted field from the driving current. These results highlight the importance of Kerr microscopy to study the current-induced motion of individual domain walls in perpendicularly magnetized wires.

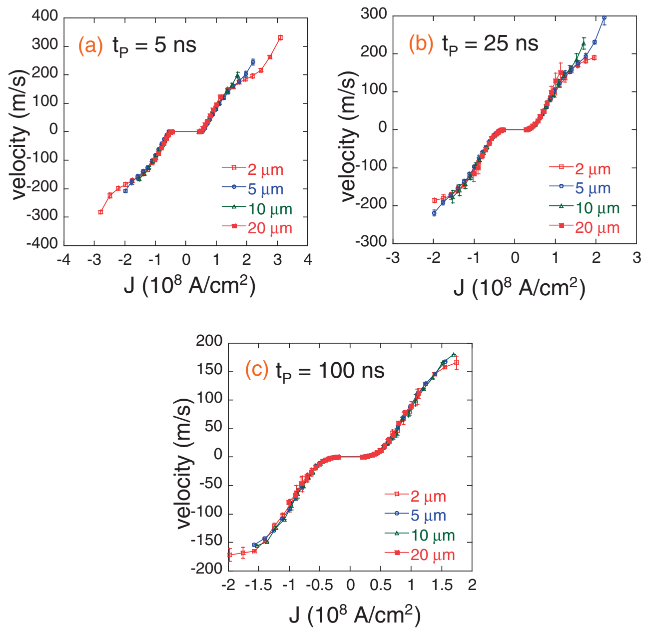

Fig. 4. DW velocity vs current density for devices having widths between 2 and 20 µm.

Acknowledgment This work was supported by the National Research Foundation of Korea Grant funded by the Korean Government (NRF-2009-352-C00029).

1) L. Berger: J. Appl. Phys. **55** (1984) 1954.
2) Z. Li and S. Zhang: Phys. Rev. B **70** (2004) 024417.
3) S. Zhang and Z. Li: Phys. Rev. Lett. **93** (2004) 127204.
4) G. Tatara and H. Kohno: Phys. Rev. Lett. **92** (2004) 086601.
5) A. Thiaville *et al.*: Europhys. Lett. **69** (2005) 990.
6) S. E. Barnes and S. Maekawa: Phys. Rev. Lett. **95** (2005) 107204.
7) J. Grollier *et al.*: Appl. Phys. Lett. **83** (2003) 509.
8) A. Yamaguchi *et al.*: Phys. Rev. Lett. **92** (2004) 077205.
9) M. Kläui *et al.*: Phys. Rev. Lett. **95** (2005) 026601.
10) M. Hayashi *et al.*: Phys. Rev. Lett. **98** (2007) 037204.
11) L. Thomas *et al.*: Science **330** (2010) 1810.
12) S. S. P. Parkin *et al.*: Science **320** (2008) 190.
13) S. Fukami *et al.*: Symp. VLSI Technology Dig. Tech. Pap., 2009, p. 230.
14) D. A. Allwood *et al.*: Science **309** (2005) 1688.
15) M. Hayashi *et al.*: Science **320** (2008) 209.
16) S.-W. Jung *et al.*: Appl. Phys. Lett. **92** (2008) 202508.
17) T. Koyama *et al.*: Nat. Mater. **10** (2011) 194.
18) I. M. Miron *et al.*: Nat. Mater. **10** (2011) 419.
19) L. Thomas *et al.*: IEDM Tech. Dig., 2011, p. 24.2.1.
20) M. Yamanouchi *et al.*: Phys. Rev. Lett. **96** (2006) 096601.
21) J. P. Adam *et al.*: Phys. Rev. B **80** (2009) 193204.
22) T. Koyama *et al.*: Appl. Phys. Lett. **98** (2011) 192509.
23) M. Yamanouchi *et al.*: Science **317** (2007) 1726.
24) K. Ando *et al.*: Phys. Rev. Lett. **101** (2008) 036601.
25) D. Chiba *et al.*: Appl. Phys. Express **3** (2010) 073004.
26) C. Burrowes *et al.*: Nat. Phys. **6** (2010) 17.